Voltage-dependent calcium channels of dog basilar artery

Elena Nikitina[1], Zhen-Du Zhang, Ayako Kawashima[1], Babak S. Jahromi[1], Vitali A. Bouryi[2], Masataka Takahashi[1], An Xie[1] and R. Loch Macdonald[1]

[1]*Section of Neurosurgery, Department of Surgery, University of Chicago Medical Center and Pritzker School of Medicine, Chicago, IL, USA*
[2]*Bogomoletz Institute of Physiology, National Academy of Sciences of Ukraine, Kiev, Ukraine*

Electrophysiological and molecular characteristics of voltage-dependent calcium (Ca^{2+}) channels were studied using whole-cell patch clamp, polymerase chain reaction and Western blotting in smooth muscle cells freshly isolated from dog basilar artery. Inward currents evoked by depolarizing steps from a holding potential of –50 or –90 mV in 10 mM barium consisted of low- (LVA) and high-voltage activated (HVA) components. LVA current comprised more than half of total current in 24 (12%) of 203 cells and less than 10% of total current in 52 (26%) cells. The remaining cells (127 cells, 62%) had LVA currents between one tenth and one half of total current. LVA current was rapidly inactivating, slowly deactivating, inhibited by high doses of nimodipine and mibefradil ($> 0.3\ \mu$M), not affected by ω-agatoxin GVIA (γ100 nM), ω-conotoxin IVA (1 μM) or SNX-482 (200 nM) and probably carried by T-type Ca^{2+} channels based on the presence of messenger ribonucleic acid (mRNA) and protein for $Ca_{v3.1}$ and $Ca_{v3.3}$ α_1 subunits of these channels. LVA currents exhibited window current with a maximum of 13% of the LVA current at –37.4 mV. HVA current was slowly inactivating and rapidly deactivating. It was inhibited by nimodipine ($IC_{50} = 0.018\ \mu$M), mibefradil ($IC_{50} = 0.39\ \mu$M) and ω-conotoxin IV (1 μM). Smooth muscle cells also contained mRNA and protein for L- ($Ca_{v1.2}$ and $Ca_{v1.3}$), N- ($Ca_{v2.2}$) and T-type ($Ca_{v3.1}$ and $Ca_{v3.3}$) α_1 Ca^{2+} channel subunits. Confocal microscopy showed $Ca_{v1.2}$ and $Ca_{v1.3}$ (L-type), $Ca_{v2.2}$ (N-type) and $Ca_{v3.1}$ and $Ca_{v3.3}$ (T-type) protein in smooth muscle cells. Relaxation of intact arteries under isometric tension *in vitro* to nimodipine (1 μM) and mibefradil (1 μM) but not to ω-agatoxin GVIA (100 nM), ω-conotoxin IVA (1 μM) or SNX-482 (1 μM) confirmed the functional significance of L- and T-type voltage-dependent Ca^{2+} channel subtypes but not N-type. These results show that dog basilar artery smooth muscle cells express functional voltage-dependent Ca^{2+} channels of multiple types.

(Submitted 5 December 2006; accepted 19 December 2006; first published online 21 December 2006)
Corresponding author R. L. Macdonald: Division of Neurosurgery, St Michael's Hospital University of Toronto, 30 Bond Street, Toronto, ON, Canada, MSB 1W8. Email: Macdonaldlo@smh.toronto.on.ca

Intracellular free calcium (Ca^{2+}) ions play a key role in the regulation of cerebral arterial smooth muscle tone under physiological conditions (Nelson *et al.* 1990; Alborch *et al.* 1995). Intracellular Ca^{2+} concentration ($[Ca^{2+}]_i$) is determined by the balance between influx of Ca^{2+} from the extracellular space and release from intracellular stores on one hand and extrusion via the plasma membrane and uptake into intracellular stores on the other. In cerebrovascular smooth muscle, Ca^{2+} influx via voltage-dependent Ca^{2+} channels is the main pathway by which $[Ca^{2+}]_i$ increases for activation of contraction (Nelson & Quayle, 1995). Ca^{2+} influx through these channels is regulated largely by the membrane potential (V_m) with depolarization increasing voltage-dependent Ca^{2+} channel open probability, elevating $[Ca^{2+}]_i$ and leading to contraction.

Voltage-dependent Ca^{2+} channels are classified into L-, T-, N-, P/Q- and R-types. These types may be distinguished by differences in voltage ranges of activation, single channel conductances and sensitivities to pharmacological agents (Yatani *et al.* 1987; Nakayama & Brading, 1993). L-, N-, P/Q- and R-type voltage-dependent Ca^{2+} channels tend to be activated at less negative voltages and thus have been referred to as high voltage-activated (HVA) Ca^{2+} channels whereas T-type channels activate at lower potentials and have been called low voltage-activated (LVA) channels. Expression of different types of voltage-dependent Ca^{2+} channels in vascular smooth muscle appears to vary with species, vascular bed and with physiological and pathological conditions.

Previous studies have suggested that normal vascular smooth muscle expresses L- (Benham *et al.* 1987; Yatani

 DOI: 10.1113/jphysiol.2006.126128

et al. 1987; Aaronson *et al.* 1988; Loirand *et al.* 1989; Nakayama & Brading, 1993), P/Q- (Hansen *et al.* 2000) and nifedipine-resistant high voltage-activated (HVA) Ca^{2+} channels (Simard, 1991; Morita *et al.* 1999). Evidence for T-type channels, which generally are low voltage-activated, is based on quite rudimentary electrophysiological data and on no molecular information. Even less is known about the electrophysiological characteristics and molecular identity of voltage-dependent Ca^{2+} channels in cerebral arteries (Alborch *et al.* 1995). There are few reports of small conductance, voltage-dependent Ca^{2+} channels in rabbit basilar artery smooth muscle but the other features were different from T-type channels (Oike *et al.* 1990; Worley *et al.* 1991). Most authors suggest that cerebrovascular smooth muscle expresses only HVA currents mediated by L-type Ca^{2+} channels (Buljubasic *et al.* 1992; Langton & Standen, 1993; Kim *et al.* 2003; Ishiguro *et al.* 2005).

Therefore, the purpose of this work was to describe voltage-dependent Ca^{2+} channel currents in dog basilar artery smooth muscle cells. We show that these cells, in addition to HVA channels, possess LVA Ca^{2+} channels of the T-type and that they have LVA Ca^{2+} currents. The LVA, in contrast to HVA, window current, was in the range of the resting V_m and may contribute to basal arterial tone and/or to spontaneous rhythmic contractions that have been observed in basilar artery (Omote & Mizusawa, 1996). We suggest that HVA Ca^{2+} current in normal cerebral arteries is mediated not only by L-type Ca^{2+} channels but also by N-type Ca^{2+} channels. Furthermore, basilar artery smooth muscle cells are shown to be heterogeneous in terms of types of voltage-dependent Ca^{2+} channel currents that are present.

Methods

Cell isolation

Experiments were conducted on smooth muscle cells harvested from the basilar arteries of adult mongrel dogs weighing 15–25 kg. Experiments were conducted in accordance with procedures for the care and use of animals established by the National Institutes of Health and followed protocols approved by the Institutional Animal Care and Use Committee of the University of Chicago. Dogs were sedated by intravenous injection of sodium pentothal (15 mg kg^{-1}) and then intubated and ventilated on oxygen and 1–2% isoflurane. They were killed under general anaesthesia by exsanguination and perfused with 8 l ice-cold phosphate-buffered saline (PBS, pH 7.4) at an intraluminal pressure of 25–30 mmHg. After perfusion, the brain was excised and placed in 4°C PBS. The endothelium was removed by passing an angiography guide wire the same size as the arterial lumen through the lumen and then flushing the artery with PBS. The basilar artery was separated from the brain and placed in ice-cold dissection solution consisting of (mM): 130 NaCl, 5 KCl, 1.3 $MgCl_2$, 10 *N*-2-hydroxyethylpiperazine-*N*′-2-ethanesulphonic acid (Hepes) and 5 glucose. Osmolarity was 300 mosmol l^{-1} and pH 7.4. Penicillin (100 U ml^{-1}) and streptomycin (0.1 mg ml^{-1}) were added to prevent bacterial contamination. Segments of artery were cleaned of surrounding connective tissue and cut into ∼1 mm square pieces, which were incubated with gentle agitation in digesting solution for 30 min at 37°C. Digesting solution was dissecting solution containing (mg ml^{-1}): 10 elastase, 1.12 collagenase type 4, 0.75 soybean trypsin inhibitor and 0.1 deoxyribonuclease-1. Following digestion, the supernatant fluid was discarded and the softened tissue was washed once in 1 ml dissecting solution containing 0.2% bovine serum albumin and triturated in 1 ml of the same solution with a wide-pore flame-polished Pasteur pipette. Cells were stored at 4°C and used within 12 h of digestion. Analysis of data obtained at different times after digestion showed no differences for cells obtained over this time and this time is comparable with that used by others (Bean *et al.* 1986; Findlay, 2002).

Patch clamp recordings

Smooth muscle cells were plated directly onto the glass bottom of the experimental chamber and visualized using an inverted microscope (Nikon, Tokyo, Japan) under phase-contrast illumination. Cells were allowed to settle for 30 min and then were washed with bath solution for 20 min to remove debris from the chamber. The bath solution contained (mM): 125 tetraethylammonium (TEA)-Cl, 5 4-aminopyridine, 1 $MgCl_2$, 10 $BaCl_2$, 10 Hepes, 0.1 ethylene glycol-bis-(b-aminoethyl ether)-*N,N,N′,N′*-tetraacetic acid (EGTA) and 10 glucose with pH 7.4 and osmolarity of 300 mosmol l^{-1}. For some experiments, Ba^{2+} was replaced with Ca^{2+} (10 mM). Voltage-dependent Ca^{2+} channel currents were isolated by eliminating K^+ currents by inclusion of Cs^+ in the patch pipette and TEA and 4-aminopyridine in the bath solution. Varying the bath concentration of Cl^- and application of the Cl^- channel antagonist, 4,4′-diisothiocyanatostilbene-2,2′-disulphonic acid, did not disclose any evidence for Cl^- conductance in these cells (data not shown). Tetrodotoxin, 1 μM, in the bath solution, also did not affect current magnitude or time course, demonstrating that recorded currents were not due to tetrodotoxin-sensitive Na^+ channels (Hollywood *et al.* 1997). Patch pipettes were filled with solution containing (mM): 130 CsCl, 1.5 $MgCl_2$, 5 Mg-ATP, 0.1 Na_2-GTP, 10 Hepes, 10 glucose and 10 EGTA with pH adjusted to 7.2 and osmolarity of 300 mosmol l^{-1}. Electrophysiological responses were tested only in those cells that were spindle-shaped, visually phase-dense with smooth and bright borders and firmly adherent to the

bottom of the chamber. These cells contracted in response to application of endothelin-1 or depolarization with KCl and showed positive immunohistochemical staining for the smooth muscle marker α-actin (data not shown).

Patch electrodes were pulled from borosilicate glass capillary tubing (1.5 mm OD, 0.86 mm ID, Sutter Instrument Co., Novato, CA, USA) with a micropipette puller (Sutter P-97, Sutter) and fire polished on a microforge (World Precision Instruments, Berlin, Germany). They had resistances of 2–3 MΩ when filled with pipette solution. An Ag–AgCl pellet connected via a 3 M KCl–agar bridge previously equilibrated in isotonic TEA-Cl solution to prevent any leak of K^+ ions into the bath solution was used to ground the bath.

Whole-cell voltage-clamp was performed using a computer-controlled current and voltage clamp system (Multiclamp 700A, 16-bit data acquisition system, Digidata 1332A, Axon Instruments, Foster City, CA, USA) driven by Clampex 8.2 and Multiclamp Commander 1 (Axon). Pipette offset, whole-cell capacitance and series resistance (to 80%, bandwidth > 5 kHz) were compensated electronically. The average access resistance was 6.00 ± 0.23 MΩ and the average cell capacitance was 24.5 ± 0.4 pF ($n = 207$ cells from 17 dogs). Current traces were filtered at 1 kHz with a low-pass 4-pole Bessel filter in the clamp amplifier, subjected to $P/4$ leak subtraction and digitized at 5 kHz before being stored on the computer hard drive for later analysis. Leak subtraction assumed no resting I_{Ba}, an assumption that may be incorrect in these cells and would mainly lead to an underestimate of the magnitude of the measured currents.

Currents through HVA and LVA Ca^{2+} channels were evaluated using Ba^{2+} (I_{Ba}) or Ca^{2+} as the charge carrier. I_{Ba} were evoked using several voltage protocols. For activation of macroscopic currents, cells were held at holding potentials of –50 or –90 mV and subjected to step depolarizations of 250 ms to –50 to +80 mV in 10 mV increments every 5 s. Data were collected after the whole-cell configuration was obtained and current amplitude had stabilized, usually ∼5 min after rupture of the cell membrane. Only cells with an input resistance > 1 GΩ with no substantial run-down were analysed. Additionally, 300–350 ms ramp voltage protocols from holding potentials of –50 or –90 mV to +80 mV were run on each cell.

To estimate the rate of Ca^{2+} channel deactivation, tail currents upon repolarization were analysed using 20–50 ms voltage steps. These data were digitized at 50 kHz and filtered at 10 kHz. Capacitance currents were removed from the analysis of tail currents by starting curve fitting after subtracting the first 2 ms or less of the tail current recording.

Voltage dependency of I_{Ba} inactivation was investigated using a double-pulse protocol with a 5 s conditioning voltage step to potentials between –100 and +40 mV in 10 mV increments. This was followed by a 5 ms interpulse to the corresponding holding potential and then by a 100 ms test pulse to –20 mV to evaluate inactivation of LVA Ca^{2+} channels or to 0 mV for HVA Ca^{2+} channels. A test pulse of 0 mV was chosen to diminish contamination of evoked currents by outward leak currents, which may become quite prominent at positive potentials. Inactivation protocols were run without leak subtraction.

Effects of Ca^{2+}-channel antagonists were tested using one 250 ms voltage step to –20 mV from a holding potential of –90 mV for LVA and –50 to +10 mV for HVA current, and ramp depolarizations from a holding potential of –90 mV. Drugs were applied to single cells with a DAD-VC superfusion system (ALA Scientific Instruments Inc., Westbury, NY, USA). The tip of the 8-line micromanifold was located within 200 μm of the tested cell, allowing exchange of the solution bathing it within a few seconds. Antagonists used were nimodipine, mibefradil, SNX-482, ω-conotoxin GVIA and ω-agatoxin IVA. Nimodipine and mibefradil were dissolved at 100 mM in dimethylsulfoxide (DMSO) and diluted to final concentrations in the bath solution. The highest concentration of DMSO in the bath solution was 0.1%, which did not affect any of the recorded currents. All experiments were performed in an air-conditioned room at ∼24°C.

Molecular biology

Total ribonucleic acid (RNA) was extracted from dog brain and enzymatically dissociated dog basilar artery smooth muscle cells with TRIzol (Gibco BRL; Life Technologies, Rockville, MD, USA). Cells from the basilar artery from which the endothelium had been removed resulted in a pure preparation of smooth muscle cell RNA. RNase-free DNase (Promega, Madison, WI, USA) was used to eliminate possible contamination of RNA preparations by traces of genomic DNA. Total RNA (1 μg) was used for reverse transcription using Superscript II and oligo dT primers (Invitrogen Life Technologies, Carlsbad, CA, USA). RNase H was used to remove the RNA template from cDNA following first-strand synthesis. Primers for polymerase chain reaction (PCR) were designed from published sequences for α_1 subunits of known Ca^{2+} channels except for $Ca_{v2.3}$ which was designed by Primer3, a web-based software program (Whitehead Institute, Massachusetts Institute of Technology, Boston, MA, USA) (Table 1; Glassmeier *et al.* 2001; Hansen *et al.* 2001; Han *et al.* 2002; D'Ascenzo *et al.* 2004). Brain served as a positive control. PCR was performed with 1 μl of reverse transcription product using a Taq PCR Master Mix Kit (Qiagen, Valencia, CA, USA).

PCR products were separated on a 1% agarose gel. Visible bands were excised and PCR products were extracted using a QIAQuick gel extraction kit (Qiagen). The extracted products were sequenced by the Gene

Table 1. Oligonucleotide primer sequences for α_1 subunits of voltage-dependent Ca^{2+} channels

Channel	Gene bank accession no.	Sense primer	Antisense primer
L-type $Ca_v1.1$ (α_{1S})	L04684	CTGGAAAGGACCAACTCTCT	TGAGCCGAATTCCTGGGAAC
L-type $Ca_v1.2$ (α_{1C})	AF465484	CCAAGAACCAGCACCAG	CCCACAACAATCAAGGC
L-type $Ca_v1.3$ (α_{1D})	DQ030979	TCCAAGATGTTCAATGACG	GTGATGGAGATTCTATTGC
P/Q-type $Ca_v2.1$ (α_{1A})	AF004884	CGAGAACAGCCTTATCGTCAC	GTGGAGAGGATGAACATGGAGC
N-type $Ca_v2.2$ (α_{1B})	M94173	GGTGAAAGCACAGAGCTTCTACTG	CCAACAGAGCGAAGACCACAATG
R-type $Ca_v2.3$ (α_{1E})	AY406056	CTCCACACTGATGGCTCTGA	GCTGCCTCTGTTTCCTTCACC
T-type $Ca_v3.1$ (α_{1G})	NM018896	CATCGTGGACAGCAAGTAC	CCAAGGATGCTGAAGATG
T-type $Ca_v3.3$ (α_{1I})	XM010005	CTCCTTCCTGCTCATCG	GTTGCAGTACTTGAGGGC

Sequencing Core Facility at the University of Chicago and matched L- ($Ca_{v1.2}$ and $Ca_{v1.3}$), P/Q- ($Ca_{v2.1}$), N- ($Ca_{v2.2}$), R ($Ca_{v2.3}$) and T-type ($Ca_{v3.1}$ and $Ca_{v3.3}$) voltage-dependent Ca^{2+} channel α_1 subunits. The accession numbers of genes that matched sequences in the gene bank are provided (Table 1).

For Western blotting, protein extracted along with mRNA using TRIzol was quantified by spectrophotometry (at 562 nm) with Micro BCA Protein Assay Reagents (Pierce Biotechnology, Rockford, IL, USA). Protein was solubilized in buffer containing 1% sodium dodecyl sulphate and 40% urea and separated on 7.5% Tris-HCl gels (Bio-Rad, Hercules, CA, USA) at 200 V for 40 min and then transferred onto nitrocellulose membranes at 100 V for 2 h. Membranes were incubated in 5% skimmed milk in Tris-buffered saline with Tween 20 (20 mM Tris-Cl, 137 mM sodium chloride, 0.1% Tween 20, pH 7.6) at 4°C overnight. Primary antibodies (1 : 200) in 2% Tris-buffered saline with Tween 20 were added for 2 h at room temperature. Primary antibodies were polyclonal rabbit IgG to $Ca_{v1.2}$, $Ca_{v1.3}$, $Ca_{v2.1,}$ $Ca_{v2.2}$, $Ca_{v2.3}$, $Ca_{v3.1}$ and $Ca_{v3.3}$ (Alomone Laboratories, Jerusalem, Israel). Membranes were then incubated with horseradish peroxidase-conjugated secondary antibody (1 : 2500) (mouse anti-rabbit IgG, Promega, Madison, WI, USA). The specific bands were detected by the enhanced chemiluminescence Plus Western blotting detection system (Amersham).

Confocal microscopy

Voltage-dependent Ca^{2+} channel α_1 subunits in basilar artery smooth muscle cells were examined by confocal imaging of enzymatically dissociated smooth muscle cells. Isolated cells were placed on poly D-lysine-coated glass coverslips and allowed to adhere for 30 min at 4°C. Samples were fixed for 15 min in PBS containing 1% paraformaldehyde and 20% sucrose and then permeabilized with 0.1% Triton X-100 for 10 min Dog serum (20%) was added for 60 min at 25°C followed by incubation with anti-Ca_v antibodies used for Western blotting at room temperature for 2 h. Secondary antibody was Alexa Fluor 488 goat IgG to the appropriate species of the primary antibody (1 : 300, Molecular Probes, Eugene, OR, USA) for 30 min at 25°C followed by 20 min incubation with rhodamine phalloidin (2.5 μg ml^{-1}, Molecular Probes) at room temperature. Cells were viewed under an Olympus 1×70 confocal microscope and the images were acquired under constant power and gain settings using FluoView software.

Isometric tension

The excised basilar artery with endothelium removed was cut into rings 3.5 mm long. Rings were mounted on metal hooks immersed in tissue baths on a custom-built tension recording system (Young *et al.* 2006). The hooks were connected to transducer arms via vertical bars with the distance between the hooks controlled by a micrometer. The baths contained Krebs-Henseleit buffer (mmol l^{-1}): NaCl 123, KCl 5.9, $CaCl_2$ 2.5, $MgSO_4$ 1.2, $NaHCO_3$ 25, KH_2PO_4 1.2 and glucose 11), bubbled with 95% O_2 and 5% CO_2, pH 7.4. Bath temperature was controlled thermostatically at 37°C. Force was measured by force measurement beams (Advanced Custom Sensors, Inc., Model 6000-c25, Irvine, CA, USA). Acquired data were sampled at 2 Hz using custom software (J. Young, University of Chicago) implemented using Igor and NiDAQ Tools 1.5 (Wavemetrics, Lake Oswego, OR, USA) running on a personal computer.

The diameter of the basilar artery *in vivo* was measured from angiograms corrected for magnification using a radio-opaque marker in each radiograph and by determination of the location of the basilar artery within the radiographic beam. For baseline adjustment of tension, artery rings were stretched to their diameter *in vivo* using the equation: $L = (\pi D - 2\pi r)/2 - 2r$ where L is the distance between the hooks, D is the diameter of the basilar artery *in vivo* and r is the radius of the hook. Rings were contracted at intervals with KCl, 60 mmol l^{-1}, until stable contractions were obtained. Relaxations from baseline were determined by addition of antagonists. Contraction–concentration curves then were generated in response to increasing concentrations of KCl in the presence and absence of each antagonist. Only one antagonist and set of manipulations were done on each ring.

Drugs

Nimodipine, mibefradil, SNX-482, ω-conotoxin GVIA, ω-agatoxin IVA, cromakalim, inorganic salts, DMSO, penicillin, streptomycin (lyophilized), 4-AP, Mg-ATP, Na_2-GTP, D-(+)-glucose, Hepes and fatty acid-free bovine serum albumin were purchased from Sigma-Aldrich (St Louis, MO, USA). TEA-Cl and EGTA were obtained from Fluka Bio Chemica (Buchs, Switzerland). Elastase, collagenase type 4, soybean trypsin inhibitor and deoxyribonuclease-1 were from Worthington Biochemical Corporation (Lakewood, NJ, USA).

Data analysis

Data were analysed with standard and custom programs in Clampfit 8.2 (Axon), Sigma Plot 8.0 (Statistical Package for the Social Sciences [SPSS], Chicago, IL, USA), Origin 6.1 (OriginLab Corp., Northampton, MA, USA) and Igor. Results are shown as mean ± standard error of the mean (S.E.M.). Student's *t* test or analysis of variance was used to determine statistical significance with $P < 0.05$ considered significant.

Results

Currents evoked from different holding potentials

Ca^{2+} currents were recorded in isolation by excluding Na^+ and K^+ from both intracellular and extracellular solutions (see Methods). Under these conditions, currents evoked by step depolarization from a holding potential of –50 or –90 mV in 10 mM Ba^{2+} solution showed voltage and time dependency characteristic of both LVA and HVA voltage-dependent Ca^{2+} channels (Fig. 1). Depolarization with 250 ms pulses from a holding potential of –90 mV revealed complete availability of voltage-dependent Ca^{2+} channels (Fig. 1*A*). Depolarization from a holding potential of –50 mV evoked currents resulting predominately from activation of HVA channels (Fig. 1*D*; Alborch *et al.* 1995; Hollywood *et al.* 2003). Each of these two families of traces shows that the peak current increased with each voltage step from –50 to +10/+20 mV and this was followed by a decline at greater depolarizations. In both cases voltage steps to +70 and +80 mV elicited small outward currents, probably due to Cs^+ efflux (Simard, 1991).

Current traces obtained in response to ramp depolarizations accentuated the difference between

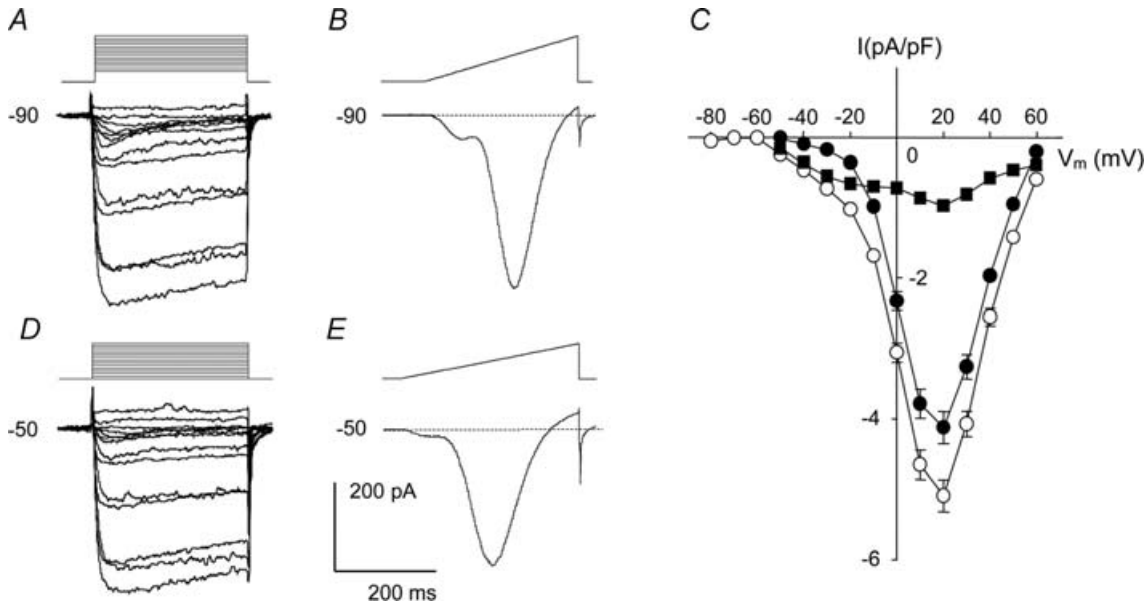

Figure 1. Voltage-dependent Ba^{2+} currents in normal dog basilar artery smooth muscle cells
A, *B*, *D* and *E*, representative examples of the most commonly found current traces recorded from single cells held at –90 mV and –50 mV. The voltage protocol is shown above each of these recordings. All 4 recordings were made from the same cell, were highly filtered for presentation purposes and are shown with the same time and current scale for comparison. *C*, summary *I–V* plots of data obtained by running step voltage protocols in 199 cells from 17 dogs held at –90 mV (○) and 207 cells from 17 dogs held at –50 mV (●). Peak inward currents were normalized to cell capacitance, averaged and plotted against step voltage (values are means ± S.E.M.). ■, the difference current obtained by subtracting the previous 2 *I–V* curves. Error bars are omitted for clarity if they were completely enveloped in the symbols. V_m is membrane potential.

currents evoked from the two holding potentials (Fig. 1*B* and *E*). Inward current at negative voltages, seen as the shoulder on the left side of the ramp current trace, was more prominent at a holding potential of –90 mV (Fig. 1*B*). This inward current was much smaller when evoked from a holding potential of –50 mV, but was still seen in the majority of cells (Fig. 1*E*), indicating that a certain number of LVA channels were still available for activation.

Dependence of I_{Ba} on V_m from initial holding potentials of –90 and –50 mV is shown as averaged current density–voltage (*I–V*) curves (Fig. 1*C*). Evoked peak currents were normalized relative to membrane capacitance and plotted as a function of the test potential. Currents elicited by step depolarizations from –90 mV were significantly larger than currents evoked by similar depolarizing steps from –50 mV at all potentials ($P < 0.01$). Inward current from a holding potential of –90 mV first appeared at a voltage step to –50 mV, while currents from a holding potential of –50 mV were first activated at –30 mV. Additional evaluation of these thresholds was estimated visually from ramp traces using only traces with clear onset of LVA and HVA components. This led to values of -51.8 ± 1.1 mV ($n = 79$ cells) and -33.1 ± 1.4 mV ($n = 17$ cells), respectively. For inactivating currents such as those observed here, however, this approach only provides an estimate of the thresholds. Both *I–V* curves reached a maximum at +20 mV and amounted to -124.4 ± 6.3 pA at a current density of -5.1 ± 0.2 A F^{-1} from a holding potential of –90 mV and -100.7 ± 6.7 pA at a current density of -4.1 ± 0.2 A F^{-1} ($n = 207$ cells from 17 dogs) from a holding potential of –50 mV.

It has been suggested that Ba^{2+} currents recorded from cells held at –90 mV can contain LVA and HVA components whereas currents elicited from –50 mV are purely HVA (Mogul & Fox, 1991; Smirnov & Aaronson, 1992). Assuming this, we attempted to confirm an LVA component by subtraction of *I–V* curves elicited at these two holding potentials, a technique previously used to separate these currents (Ohya & Sperelakis, 1989; Gordienko *et al.* 1994; Petkov *et al.* 2001). In smooth muscle cells from dog basilar artery, however, the resulting curve was not pure LVA current but demonstrated a residual HVA component which can be seen as a hump that is maximal at +20 mV (Fig. 1*C*). Only partial inactivation of HVA channels at a V_m of –50 mV could account for this residual current. The subtraction curve revealed peak LVA current at a V_m between –20 (–0.79 A F^{-1}) and –10 mV (–0.83 A F^{-1}). These results demonstrate, in contrast to some reports (Yatani *et al.* 1987; Benham *et al.* 1987), that separation of the two current components is not possible by this method in these cells (Aaronson *et al.* 1988). Changing to a holding potential of –40 mV did not improve the current separation. The left shoulder hump of the ramp traces was not eliminated but was just reduced in size (data not shown).

Heterogeneity of cells

The proportion of LVA and HVA current components evoked by depolarizing steps from –90 mV varied significantly between cells. In 24 of 203 cells (12%) from 14 dogs, LVA current formed more than 50% of the maximal current (Fig. 2*A* and *B*). An explicit criss-cross pattern, which is characteristic of T-type Ca^{2+} channels (Perez-Reyes, 2003), was seen in current recordings from cells of this type. In another group of 52 cells (26%), LVA current was less than 10% of maximal current. There were cells ($n = 5$, 3%) in which ramp current traces evoked

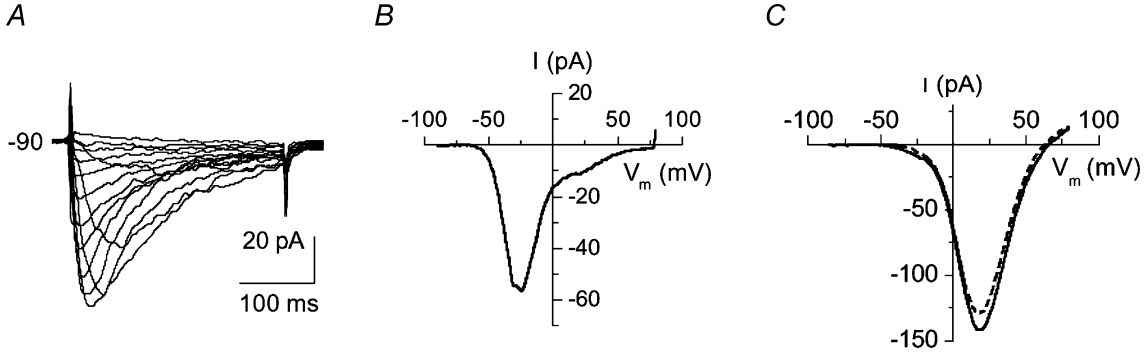

Figure 2. Normal dog basilar artery smooth muscle cells are diverse in terms of proportion of LVA and HVA currents

A, family of current traces obtained in one cell showing almost complete absence of HVA current. *B*, ramp tracing from the same cell from a holding potential of –90 mV. *C*, superimposed ramp current traces from one cell held at –90 (continuous line) and –50 mV (dotted line) plotted as current–voltage relation showing an example of virtually complete absence of the LVA current component. The difference in peak amplitudes of these 2 recordings might be attributed to different degrees of Ca^{2+} channel inactivation caused by difference in steepness/velocity of voltage changes of protocols employed and different initial holding potentials.

from holding potentials of –50 and –90 mV were almost indistinguishable (Fig. 2*C*). The remaining cells ($n = 127$, 62%) had LVA current between 10 and 50% of the HVA maximal current.

Temporal characteristics of macroscopic current

Build-up and decay of the evoked current depended on V_m. Build-up of macroscopic current became faster and decay slower with an increase in membrane depolarization (Figs 1*A* and *D*, and 2*A*). The rise phases of I_{Ba} could be adequately described by single exponents with time constant (τ_R) declining from 77.4 ± 9.2 ms for a step from –90 to –50 mV, to 2.86 ± 0.14 ms for a step to +20 mV ($n = 147$ cells from 14 dogs, data not shown). Inactivation of I_{Ba} in cells with a high proportion of LVA current developed faster than in cells with more balanced components of LVA and HVA current (compare traces in Figs 1*A* and 2*A*). The inactivation/fall phase of the 250 ms current traces required from two exponents at the most negative potentials to six (maximum number available in Clampfit) at maximal peak currents to obtain a satisfactory fit. In some cases even six exponents were not adequate. Therefore, we fitted conditioning 5 s traces from a holding potential of –90 mV to a double exponential equation ($n = 38$ cells from 4 dogs, data not shown). Values of $\tau_{F1} = 1244 \pm 81$ and $\tau_{F2} = 164 \pm 9.5$ ms for maximal peak current at a step to +20 mV were obtained. The presence of multiple Ca^{2+} channel types in these cells means that these values are averages only and do not reflect intrinsic features of the participating channels.

Data above suggest there was a component of I_{Ba} with characteristics of a LVA current based on its low activation threshold, fast inactivation kinetics and criss-cross current pattern. Another feature of LVA Ca^{2+} channels is slow deactivation (Kim *et al.* 2002; Perez-Reyes, 2003). We examined the deactivation kinetics of I_{Ba} by applying voltage steps of 20 or 50 ms duration, which were long enough to evoke peak current while avoiding visible inactivation. Repolarization from these steps back to the holding potential induced tail currents with relatively slow decay (Fig. 3*A* and *B*). Deactivation decay to the holding

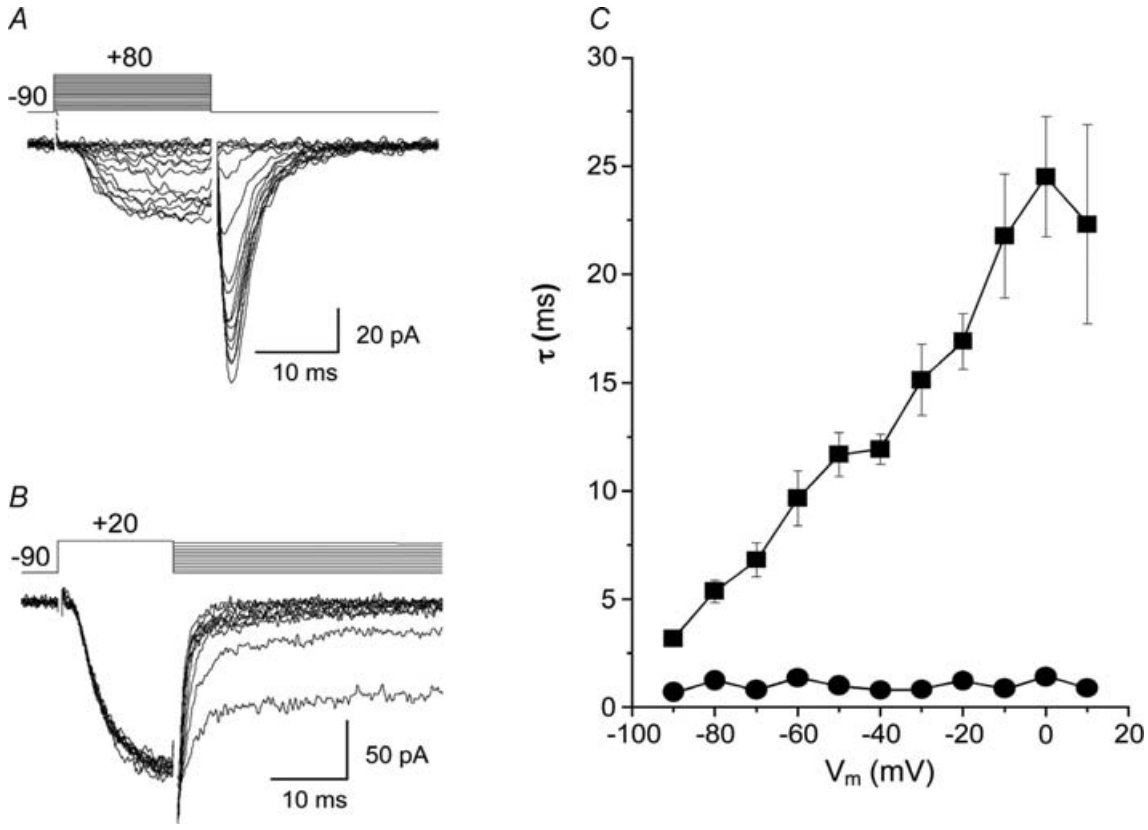

Figure 3. Tail currents in dog basilar artery smooth muscle cells
A, representative recordings of tail currents obtained by running the step voltage protocol shown above the traces with a test pulse duration of 50 ms. *B*, voltage dependence of Ca^{2+} channel deactivation was revealed from tail currents evoked by a 20 ms test voltage pulse from –90 mV to +20 mV to evoke maximal I_{Ba} with subsequent return to different potentials (–90 to +10 mV in 10 mV increments). *C*, the decline of tail currents was described by a double exponential function. Averaged values of time constants (τ) obtained from such fitting and plotted against after-pulse potentials showed quite different behaviour. The smaller τ was voltage independent (●) while larger τ showed linear voltage dependency (■) with a slope factor of 0.23 s V^{-1} ($n = 14$ cells from 4 dogs).

potential of –90 mV could be described well by a double exponential function with time constants τ_1 of 5.51 ± 0.61 and τ_2 of 1.02 ± 0.22 ms ($n = 14$ cells from 4 dogs) for peak currents. Voltage dependence of the larger deactivation τ was revealed by the voltage protocol (top of Fig. 3*B*) showing the deactivation τ obtained from exponential fitting of repolarization curves grew linearly e times for every 28.3 mV increase in repolarization potential (Fig. 3*C*). The smaller τ did not change significantly. The findings were the same when beginning from a holding potential of –50 mV.

I_{Ba} inactivation and window currents

Prolonged depolarization elicited inactivation of I_{Ba} in dog basilar artery smooth muscle cells. To assess the voltage dependence of steady-state inactivation, a standard double-pulse protocol was employed (Fig. 4*A*

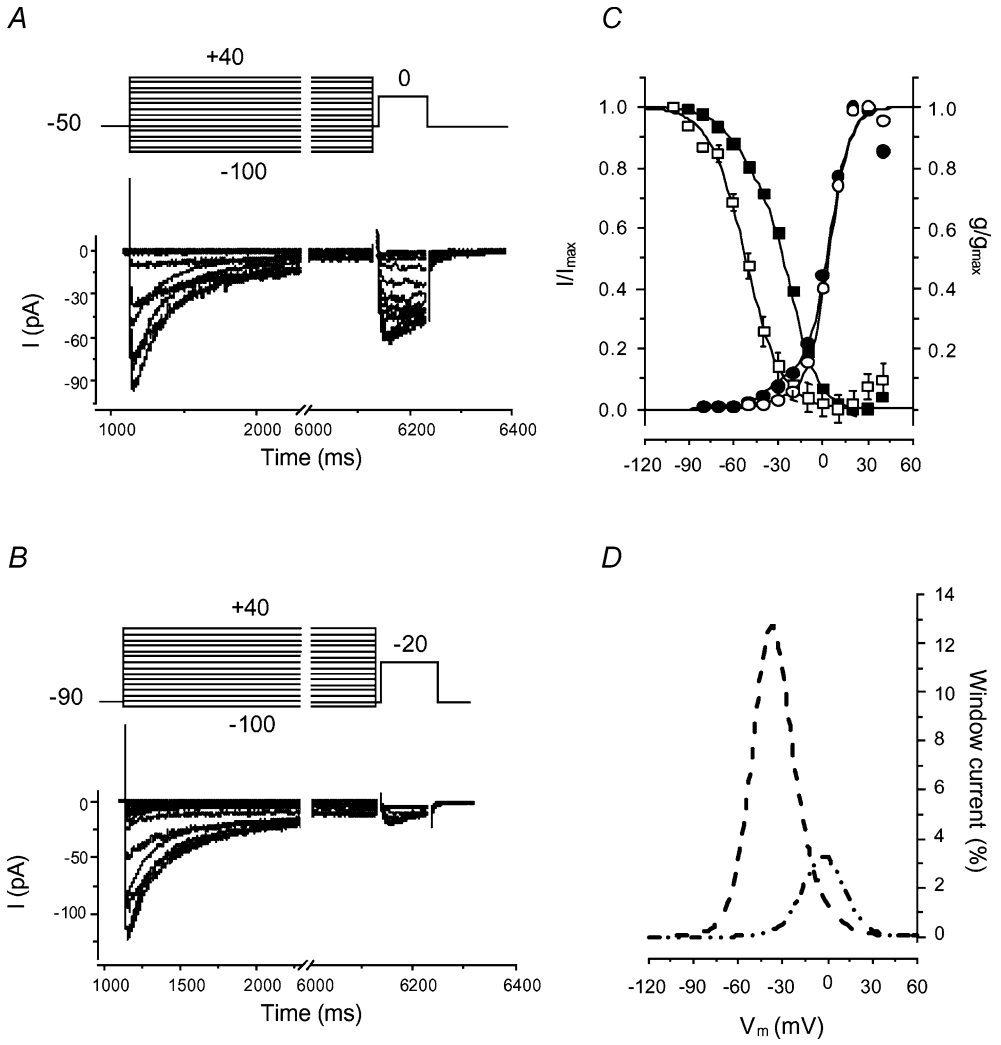

Figure 4. Activation–inactivation characteristics of HVA and LVA components of I_{Ba} and window currents in dog basilar artery smooth muscle cells

A and *B*, typical series of current traces obtained from a single cell by stepping to 0 mV (*A*) or –20 mV (*B*) for 100 ms following application of a series of 5 s conditioning potentials from –100 mV to +40 mV in 10 mV increments with a 5 ms interpulse (upper parts of panels show schematics of voltage protocols). *C*, summary data demonstrating the voltage dependence of I_{Ba} inactivation (squares) and activation (circles). ■, total availability of Ca^{2+} channels ($n = 42$ from 4 dogs) and the curve is the fit to a double Boltzmann equation. □, availability of LVA channels fitted to single Boltzmann equation ($n = 35$ from 4 dogs). Voltage dependence of activation was derived from data shown in Fig. 1. ●, total inward current from a holding potential of –90 mV; and ○, HVA current from a holding potential of –50 mV. Both sets of data were fitted to double Boltzmann equations with curves showing the fits. *D*, the LVA and HVA components of mathematical activation and inactivation models were normalized to their maximal amplitudes and multiplied in pairs giving percentile *I–V* curves for window currents through LVA (dashed line) and HVA (dash–double dot line) channels.

and B). For each cell, steady-state inactivation (availability) was evaluated as an I/I_{max} ratio plotted against the conditioning voltage where I is the current recorded and I_{max} is the maximal current elicited by a test voltage step. Data were fitted to equation:

$$I/I_{max} = A/(1 + \exp[V - V_{1i}]/k_{1i}) + (1 - A)/(1 + \exp[V - V_{2i}]/k_{2i})$$

where V is the command voltage, V_{1i} and V_{2i} are potentials of half-maximal inactivation ($V_{0.5}$), k_{1i} and k_{2i} are the slope factors and A is the relative amplitude of the respective current. We thus obtained two inactivation curves for each cell (Fig. 3C). As a rough estimate, 90% of LVA/HVA channel inactivation occurred between –72.5 and +2.5 mV and between –87.3 and –16.7 mV for LVA current.

Steady-state activation data were derived from current–voltage relationships (Fig. 1C). Conductance (G) was calculated from the equation:

$$G = I/(E_m - E_{rev})$$

where I is the peak current elicited by the depolarizing test pulse and E_{rev} is the reversal potential for the current under study. The reversal potentials were derived from iterative fitting of the original I–V curves of each cell to a Boltzmann model, giving 57.2 ± 0.6 mV for a holding potential of –50 mV and 58.7 ± 0.6 mV for –90 mV ($n = 207$ and 199 cells, respectively, from 17 dogs). The points for G/G_{max} were plotted against the membrane test potential as the relative amplitude and fitted to the sum of two Boltzmann components:

$$G/G_{max} = A/(1 + \exp[-(V - V_{1a})]/k_{1a}) + (1 - A)/(1 + \exp[-(V - V_{2a})]/k_{2a})$$

where the parameters are identical to those for the inactivation curves (potentials of half-maximal activation and slope coefficients of activation). This yielded two curves overlapping with the inactivation curves (Fig. 4C). Parameters for the activation and inactivation curves were optimized to obtain satisfactory fits with the same values for $V_{0.5}$ and k for data obtained at the different holding potentials ($V_{1i} = -52$ mV, $k_{1i} = 12$, $V_{2i} = -20$ mV, $k_{2i} = 8.6$, $V_{1a} = -38$ mV, $k_{1a} = 7$, $V_{2a} = 3$ mV, $k_{2a} = 6.5$). This allowed us to divide each data set, which consisted of a mixture of two different currents, into its components. Normalization to their maximal values and multiplication in pairs revealed window currents with peak values of 13% of maximal current at –37.4 mV for LVA and 9% at –2.25 mV for HVA currents (Fig. 4D).

We recognize that this method of quantification of voltage dependence of activation has limitations (Sun *et al.* 2000). However, it is the most widely used method for such quantification, which allows comparison of our data to that of others. Quantification of inactivation is also based on whole-cell current, which is a commonly used and accepted method. Finally, the activation parameters obtained from single channel or approximated/extrapolated tail current recordings for currents apparently carried by channels of at least four different types will not reflect true values because of the exponential growth in the number of assumptions in the models.

Calcium currents

Currents recorded in bath solution containing $[Ca^{2+}]_o = 10$ mM differed from Ba^{2+} currents in several ways. They had lower peak amplitudes at positive potentials and the ratio of LVA/HVA component amplitudes was much higher in keeping with selectivity of L-type Ca^{2+} channels for Ba^{2+} (Fig. 5). Currents inactivated faster ($\tau_1 = 177 \pm 50$ ms and $\tau_2 = 32 \pm 7$ ms) and almost completely during 400 ms test pulses (Fig. 5A) due to Ca^{2+}-dependent inactivation of L-type Ca^{2+} channels. Other temporal characteristics did not change. Activation began at -51 ± 1.0 mV (estimated from ramp recordings from –90 mV, $n = 5$) and was as rapid as Ba^{2+} current ($\tau = 2.0 \pm 0.4$ and 2.7 ± 0.1 ms, respectively, $P > 0.05$, $n = 5$). There also was no significant effect on the rate of deactivation ($\tau_1 = 9.3 \pm 2.4$ and $\tau_2 = 1.3 \pm 0.3$ ms, $P > 0.05$, $n = 5$).

Pharmacological characterization of I_{Ba}

The electrophysiological data suggest the presence of HVA and LVA Ca^{2+} channels. Therefore, we next used pharmacological antagonists of different voltage-dependent Ca^{2+} channels to characterize the channels present. Figure 6A shows a series of recordings of I_{Ba} evoked by voltage steps from a holding potential of –50 to +10 mV obtained from one cell before and after cumulative applications of nimodipine. There was progressive inhibition of peak as well as sustained current and increasingly rapid inactivation with increasing concentrations of nimodipine. Blockade was not complete (on average it was 96% with nimodipine, 10 μM) but showed a tendency towards saturation. The same cell held at –90 mV and stepped to –20 mV responded with a small LVA current that also was suppressed by high concentrations (> 0.03 μM) of nimodipine (Fig. 6B). Note that the rate of decline of the control trace also is slower than the trace recorded with nimodipine, which suggests some activation of HVA channels by the applied voltage step. The highest concentration of nimodipine (10 μM) diminished LVA current by 48%. Low concentrations of nimodipine (0.01–0.03 μM) showed a characteristic agonist effect on LVA channel current (Aaronson *et al.* 1988).

Cumulative nimodipine dose–response curves for LVA and HVA components of I_{Ba} had a complex shape, probably resulting from incomplete separation of LVA and HVA components and atypical excitation effect of the antagonist on the LVA component of I_{Ba}. These curves required equations with at least three exponents for fitting. This led to some uncertainty with regard to the fits obtained so only a graphical estimation of the IC_{50} for nimodipine inhibition of the LVA and HVA components was made. Values of 11.3 and 0.018 μM, respectively, were obtained (Fig. 6*C*).

Mibefradil, a putative specific antagonist of T-type, LVA Ca^{2+} channels, was not particularly selective (Fig. 6*D* and *E*). Analysis of current traces obtained as for nimodipine but using mibefradil show that the latter inhibited both components of I_{Ba} almost equally (Fig. 6*F*). Only traces obtained after application of mibefradil in quite high concentrations (> 3 μM) show that the remaining current inactivated slower than control, suggesting more or less complete block of typically rapidly inactivating LVA current (most of the HVA channels would be blocked under these conditions as well). Low concentrations of mibefradil also exhibited an agonist effect on LVA current (Fig. 6*E* and *F*). Mibefradil, 10 μM, suppressed about 98% of HVA and 88% of LVA current. Graphical estimates of IC_{50} values for LVA and HVA currents were 2.2 and 0.39 μM, respectively. Therefore, mibefradil was ~5-fold more potent whereas nimodipine was ~637-fold more potent at inhibiting HVA compared with LVA current.

Effects of both nimodipine and mibefradil are known to be voltage, state and use dependent (Bezprozvanny & Tsien, 1995; Jensen *et al.* 2004). Since the step protocols by which HVA and LVA currents were isolated had different holding potentials (–50 and –90 mV, respectively), the 637-fold higher potency of nimodipine against HVA current component might be an over- or underestimate (Cohen & McCarthy, 1987; McCarthy & Cohen, 1989; Hille, 2001). Therefore, we calculated potency of both drugs from data obtained from ramp voltage protocols from a holding potential of –90 mV in the absence and presence of nimodipine or mibefradil at the same range of concentrations in the bath solution (data not shown). Under these conditions, the IC_{50} for nimodipine on LVA current was 4.7 μM compared with 0.026 μM on HVA

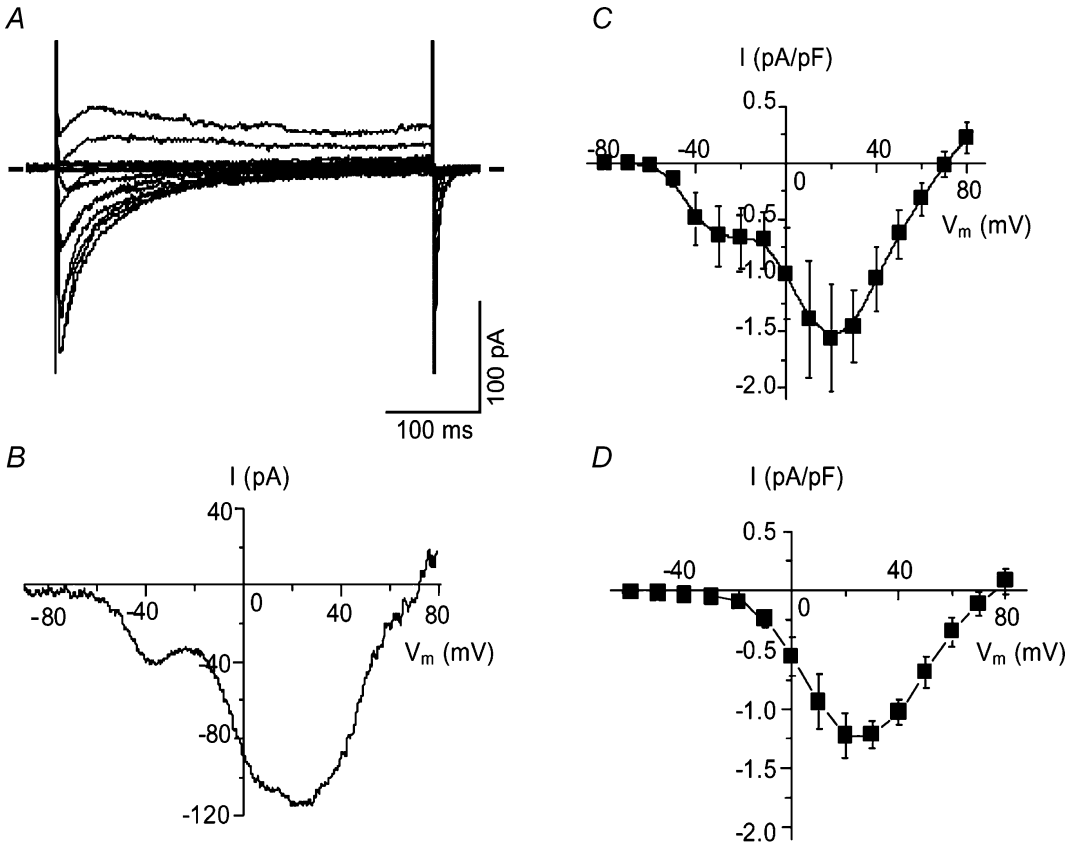

Figure 5. Voltage-dependent Ca^{2+} channel currents in normal dog basilar artery smooth muscle cells
A, Ca^{2+} current traces recorded from the cell held at –50 mV. *B*, current recorded from the same cell in response to ramp pulse from –90 to +80 mV. *C* and *D*, current–voltage relationships from step protocol data at holding potentials of –90 mV (*C*) and –50 mV (*D*) averaged from 5 cells.

current, for a relative potency of ∼179-fold higher. The IC_{50} values for mibefradil were 1.9 μM for LVA and 1.5 μM for HVA current components, confirming the relatively poor specificity in these cells.

In order to gain more information from the pharmacological data, we analysed currents elicited by ramp pulses by a different method (Fig. 7). Ramp current traces from a holding potential of –90 mV in the presence or absence of varying concentrations of nimodipine or mibefradil were averaged (20 and 13 cells from 7 dogs, respectively) and normalized point by point to the control curve which becomes a straight line at $y = 1$. We reasoned that if all channels undergoing blockade had the same affinity for the antagonist, and were therefore of the same type, then one could expect to obtain another straight line at some other constant value of $y < 1$ for each concentration of drug. If drug effect was voltage, state and/or use dependent, then the line obtained in this way should have some constant slope and be described by a linear equation. The curves obtained deviated substantially from straight lines and showed several extrema which would suggest different levels of antagonism. Low concentrations of nimodipine (0.01 μM) or mibefradil (0.01 μM) augmented currents evoked at membrane potentials below –10 and –30 mV, respectively, and inhibited currents at more positive potentials. Higher concentrations of both antagonists showed similar patterns, showing greater antagonism of currents activated below –35 mV and above –10 mV. A notable difference was

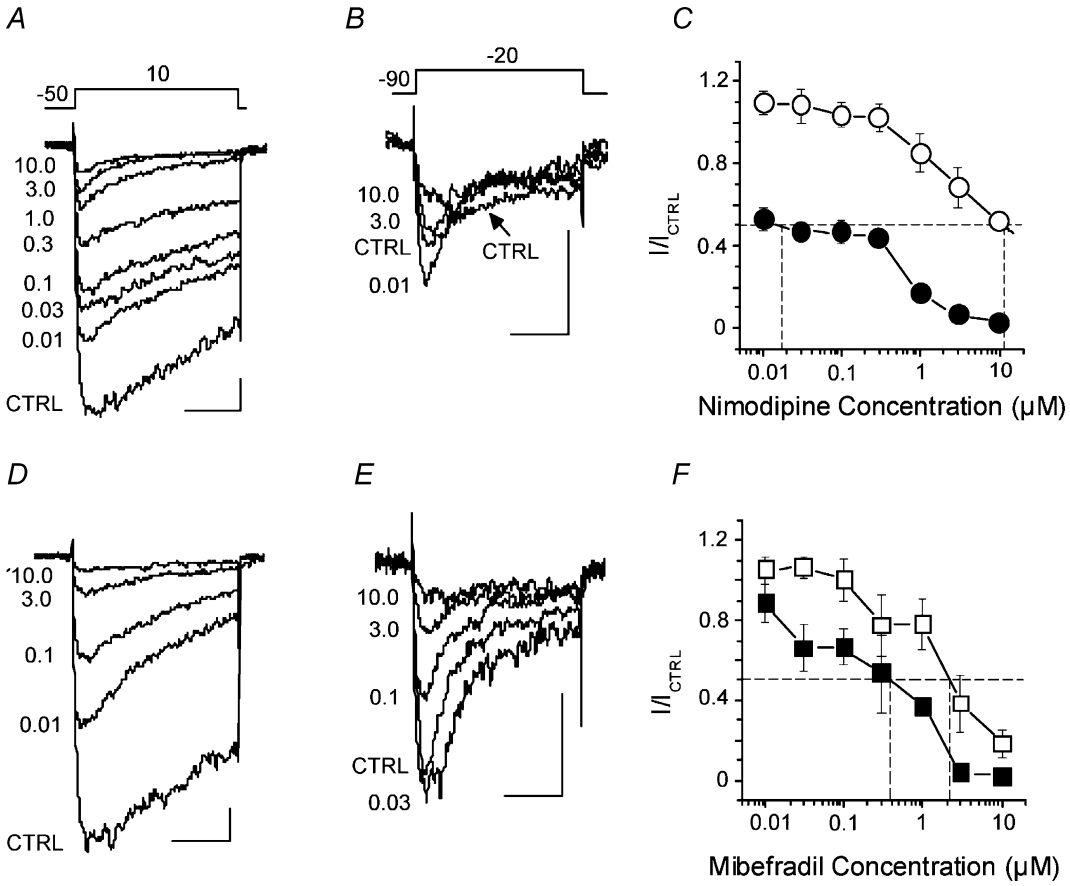

Figure 6. Nimodipine and mibefradil antagonism of voltage-dependent Ca^{2+} channel currents in freshly isolated dog basilar artery myocytes

A and *B*, representative current recordings obtained from one cell by applying voltage protocols shown above traces (in mV) before (CTRL) and after addition of different concentrations (0.01–10 μM) of nimodipine to the bath solution. *C*, averaged dose–response curves from experiments in *A* and *B* ($n = 20$ cells from 7 dogs). The points of intersection of the experimental curves with the dashed line at $y = 0.5$ give estimates of IC_{50} for LVA (○) and HVA (●) Ca^{2+} currents. *D* and *E*, representative current traces obtained from another smooth muscle cell in the absence (CTRL) and presence of mibefradil (0.01–10 μM). *F*, mibefradil dose–response curves for LVA (□) and HVA (■) Ca^{2+} channel currents ($n = 13$ cells from 7 dogs). The intersection of the experimental curves with the dashed line at $y = 0.5$ gives estimates of IC_{50} for LVA (□) and HVA (■) Ca^{2+} currents. Scale indicators in *A*, *B*, *D* and *E* are 50 ms (horizontal) and 20 pA (vertical).

that mibefradil differentiated HVA current into a component with maximal current at 0 mV with a high affinity for antagonism and a less sensitive component at +23 mV. This analysis suggested there were different populations of channels activated in three different ranges (below –35 mV, –35 to –10 mV and above –10 mV) with different sensitivities to nimodipine and mibefradil.

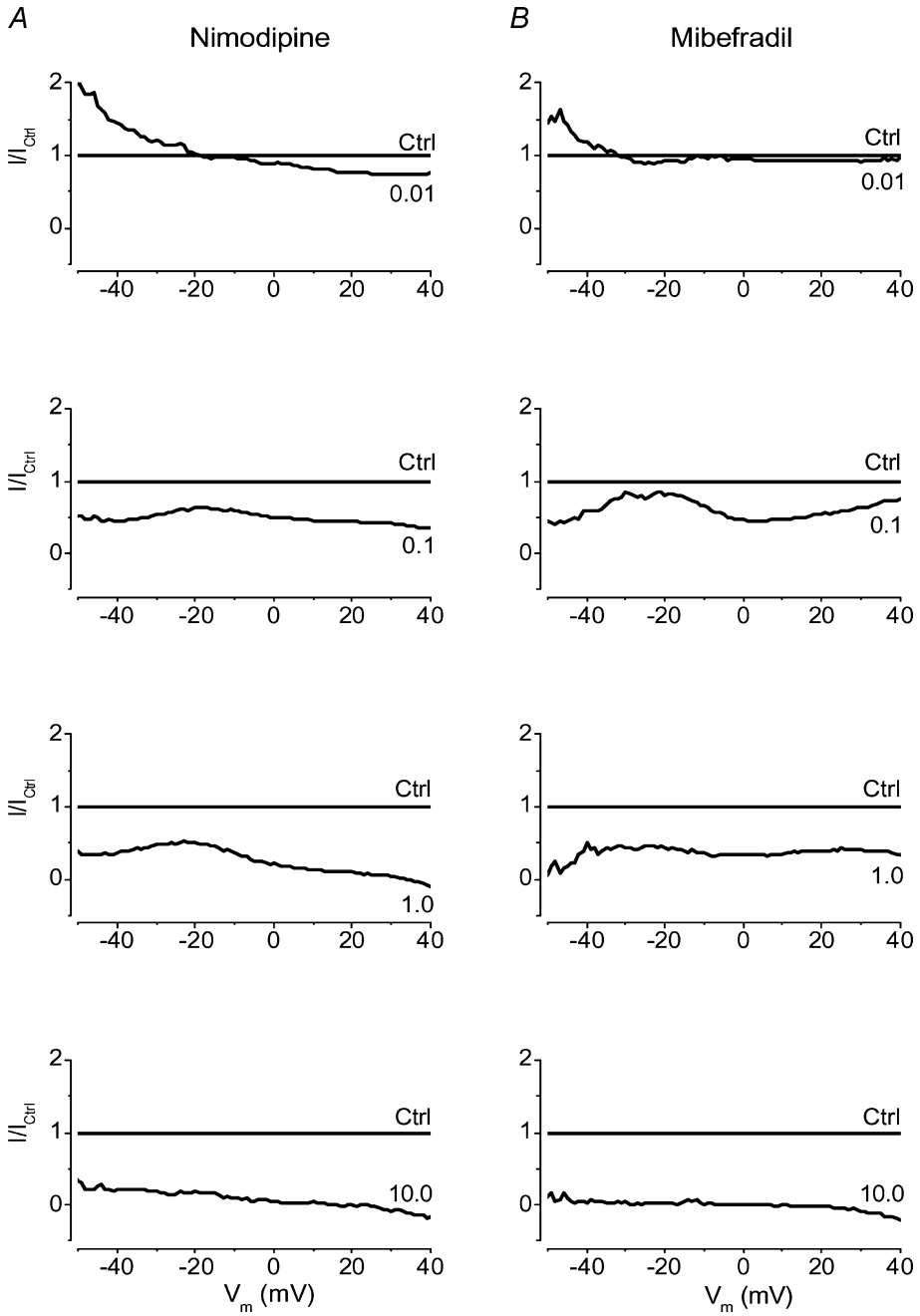

Figure 7. Analysis of current–voltage relationships for Ca^{2+} channel currents in dog basilar artery smooth muscle cells under cumulative block by nimodipine (*A*) or mibefradil (*B*)
Each curve of the upper panels represents current–voltage relationships for ramp protocol data from a holding potential of –90 mV obtained in the absence (CTRL) or presence of nimodipine (0.01–10 μM (concentration indicated on the curve in each panel), $n = 20$ cells from 7 dogs) or mibefradil (0.01–10 μM, $n = 13$ cells from 7 dogs). Data were analysed by first averaging the original data points for each mV. Each smoothed *I–V* curve then was normalized to its peak current. Normalized data for groups were averaged (bottom row) and divided point by point by the control data (dashed curve). This yielded a line at $y = 1$ (CTRL in the upper row of panels) representing the *I–V* data in the absence of any antagonist. The curves of different shapes and positions represent *I–V* data recorded at the marked concentrations of nimodipine or mibefradil.

The types of channels present were further defined using specific antagonists of other types of HVA Ca^{2+} channels (ω-agatoxin IVA, 100 nM for P/Q-, ω-conotoxin GVIA, 1 μM for N- and SNX-482, 200 nM for R-type). The voltage protocol was a ramp pulse from a holding potential of –90 mV applied every 10 s before and after addition of the antagonist. Maximal amplitudes of inward currents at voltages below –10 and above 0 mV were measured and considered to represent LVA and HVA currents. Results were averaged and expressed as a percentage of the same cell's response before drug application. These antagonists had no significant effects on LVA currents. ω-Conotoxin GVIA (γ1 μM) significantly inhibited HVA current to 83 ± 3% of control (21 cells from 5 dogs, $P < 0.05$, paired t test), suggesting the presence of a small component of N-type voltage-dependent Ca^{2+} channel current. There was a small effect of ω-agatoxin IVA (100 nM, 91 ± 3%, 21 cells from 5 dogs) that probably reflects non-specific effects. SNX-482, an R-type channel antagonist, did not alter voltage-dependent Ca^{2+} channel currents (98 ± 1% of control, 19 cells from 5 dogs, $P > 0.05$).

Molecular biology and immunohistochemistry

Basilar artery smooth muscle cells isolated from dogs contained mRNA for L- ($Ca_{v1.1,}$ (not shown), $Ca_{v1.2}$ and $Ca_{v1.3}$), N- ($Ca_{v2.2}$) and T-type ($Ca_{v3.1}$ and $Ca_{v3.3}$) voltage-dependent Ca^{2+} channel α_1 subunits (Fig. 8*A*). There was no mRNA for P/Q- ($Ca_{v2.1}$) or R-type ($Ca_{v2.3}$) α_1 subunits. Western blotting was consistent with this in that protein for L- ($Ca_{v1.2}$, $Ca_{v1.3}$), N- ($Ca_{v2.2}$) and T-type (Cav3.1 and $Ca_{v3.3}$) α_1 subunits was detected (Fig. 8*A*). The presence of endothelial and neuronal cell contamination was excluded by PCR showing no mRNA for CD31 (endothelial cells) or microtubule-associated protein 2 (MAP2, neurons, Fig. 8*C*). These data correspond to electrophysiological results that suggest the presence of LVA currents that are mediated generally by T-type and possibly $Ca_{v1.3}$ channels (Platzer *et al.* 2000) and HVA currents that are complex and mediated by L- ($Ca_{v1.2}$ and $Ca_{v1.3}$) and N- ($Ca_{v2.2}$) α_1 subunits. These results were confirmed by confocal microscopy of isolated smooth muscle cells that demonstrated the same proteins within smooth muscle cells (Fig. 8*B*).

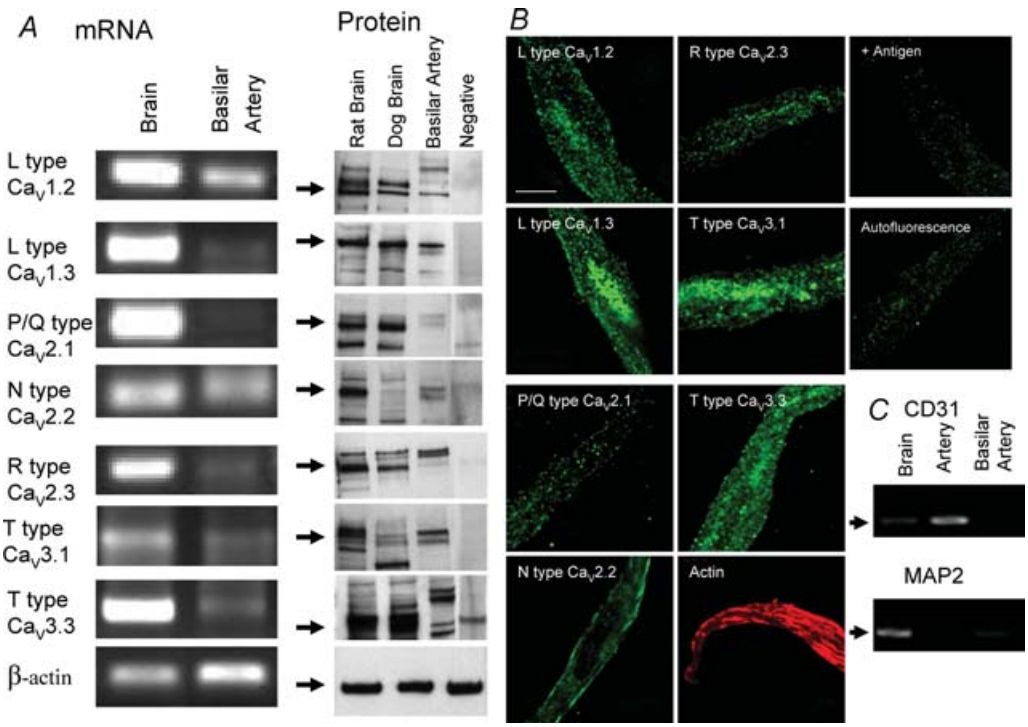

Figure 8. Messenger RNA and protein for Ca^{2+} channel α_1 subunits detected in dog basilar artery smooth muscle cells

A, PCR products from mRNA amplification of isolated basilar artery smooth muscle cells detected mRNA for L- ($Ca_{v1.2}$ and $Ca_{v1.3}$), N- ($Ca_{v2.2}$) and T-type ($Ca_{v3.1}$, $Ca_{v3.3}$) Ca^{2+} channel α_1 subunits but not P/Q- ($Ca_{v2.1}$) and R- ($Ca_{v2.3}$) subunits. Western blotting showed protein for L- ($Ca_{v1.2}$ and $Ca_{v1.3}$), N- ($Ca_{v2.2}$) and T-type ($Ca_{v3.1}$, $Ca_{v3.3}$) Ca^{2+} channel α_1 subunits. *B*, confocal microscopy of isolated smooth muscle cells was consistent with Western blotting, demonstrating positive staining for L- ($Ca_{v1.2}$ and $Ca_{v1.3}$), N- ($Ca_{v2.2}$) and T-type ($Ca_{v3.1}$, $Ca_{v3.3}$) but not P/Q- or R-type Ca^{2+} channel α_1 subunits (scale bar, 50 μM). +Antigen is control example of loss of staining for $Ca_{v1.2}$ when antibody was added with immunizing antigen. Autofluorescence also is shown. *C*, cells studied were smooth muscle cells not contaminated by endothelial cells or neurons as shown by negative PCR for CD31 and MAP2.

Isometric tension

The basilar artery was stretched under isometric tension to the equivalent of its diameter *in vivo*. Relaxation from this level, which would be equal to basal tone *in vivo*, occurred in response to nimodipine (1 μM) and mibefradil (10 μM, $P < 0.05$ for both) whereas there was no relaxation to ω-agatoxin IVA (0.4 μM), ω-conotoxin GVIA (2 μM) and SNX-482 (0.2 μM, Fig. 9*A*). Next, concentration–contraction responses to KCl were performed and were significantly inhibited by nimodipine (1 μM) and mibefradil (10 μM) but not ω-agatoxin IVA (γ0.4 μM), ω-conotoxin GVIA (2 μM) and SNX-482 (0.2 μM, Fig. 9*B* and *C*). Finally, to accentuate T-type LVA channel effects, rings were incubated with cromakalim (5 μM) in order to open ATP-dependent K^+ channels and hyperpolarize the smooth muscle cells (Fig. 9*D*). Concentration–contraction responses to KCl were then obtained in the presence or absence of nimodipine (1 μM). This demonstrated a small nimodipine-insensitive contraction at low concentrations of KCl, consistent with LVA channel function.

Discussion

This is the first study to examine the electrophysiology, pharmacology and molecular biology of voltage-dependent Ca^{2+} channels in normal dog basilar artery smooth muscle cells. There are two important, novel findings. First, these cells possess L-, N- and T-type voltage-dependent Ca^{2+} channels. Second, the basilar artery smooth muscle cells are heterogeneous in that there were cells exhibiting mostly LVA current, others with predominately HVA current and some cells with both currents.

Cerebrovascular smooth muscle cells have been suggested to possess HVA and LVA Ca^{2+} channels (Oike *et al.* 1990; Worley *et al.* 1991; Buljubasic *et al.* 1992; Langton & Standen, 1993; Kim *et al.* 2003; Ishiguro *et al.* 2005). Results have been conflicting, however, possibly because investigators have studied freshly isolated cells from different species, vascular beds and sizes of arteries as well as cultured cells in some cases (Worley *et al.* 1991; Simard, 1991; Buljubasic *et al.* 1992; Smirnov & Aaronson, 1992; Langton & Standen, 1993; Kuga *et al.*

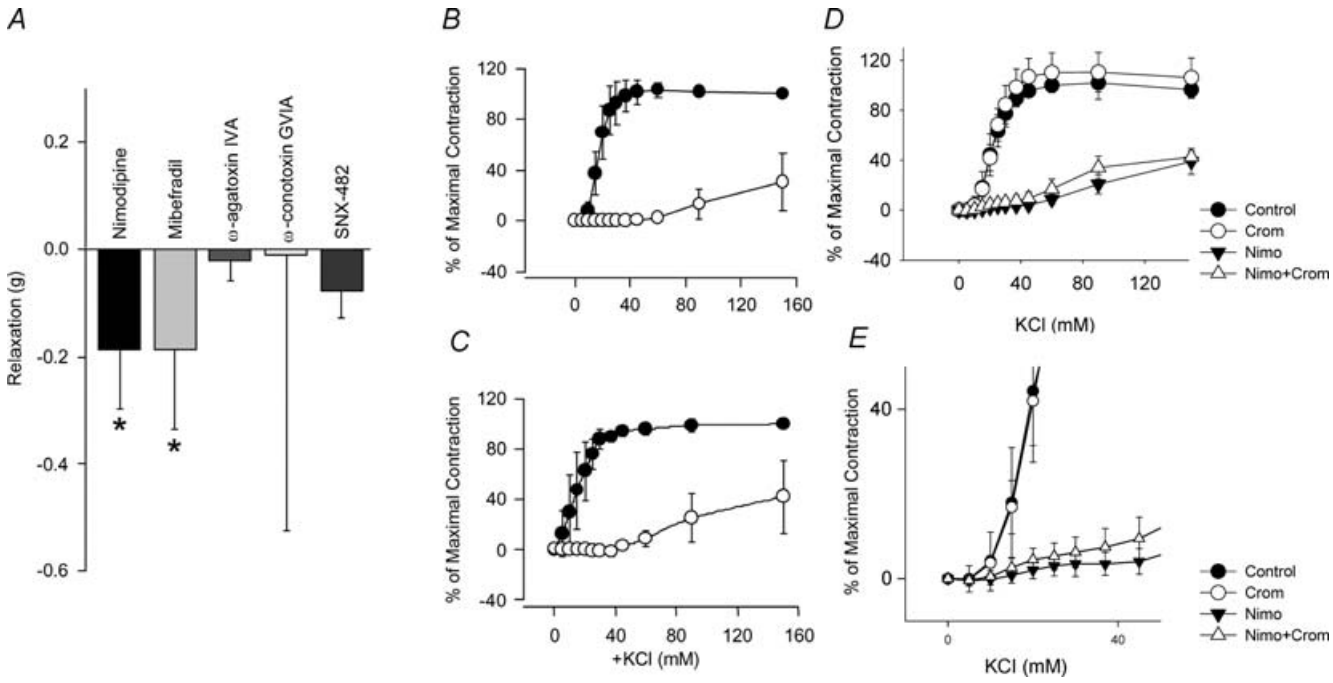

Figure 9. Isometric tension recordings showing function of Ca^{2+} channel subtypes in dog basilar artery
A, relaxation of basilar artery from baseline tension occurred in response to mibefradil (10 μM) and nimodipine (1 μM, $P < 0.05$ for both) but not to ω-agatoxin IVA (0.4 μM), ω-conotoxin GVIA (2 μM) or SNX-482 (0.2 μM). KCl concentration–contraction curves in absence (●) or presence (○) of nimodipine (*B*, 1 μM) and mibefradil (*C*, 10 μM) show significant inhibition of contraction by both drugs. *D*, KCl concentration–contraction curves in absence or presence of nimodipine (Nimo, 1 μM) or cromakalim (Crom, 5 μM) shows a small component of contraction at low concentrations of KCl not inhibited by nimodipine in the presence of cromakalim (*E*, $n = 4$–5 rings from 2 dogs for all experiments).

1996; Day *et al.* 1998; Hansen *et al.* 2001; Gustafsson *et al.* 2001). Several investigators suggested there was only L-type current in rat basilar (Langton & Standen, 1993; Simard *et al.* 1998) and dog (Buljubasic *et al.* 1992) and rabbit middle cerebral artery (Kim *et al.* 2003). In some cases experiments were conducted only from a holding potential of –60 mV so the presence of LVA current could not be determined (Buljubasic *et al.* 1992; Kim *et al.* 2003). Other studies of voltage-dependent Ca^{2+} channels in rabbit basilar artery incompletely characterized LVA current (Oike *et al.* 1990) or found channels with low unitary conductance characteristic of T-type channels but with other features of L-type Ca^{2+} channels (Worley *et al.* 1991). Molecular characterization was never carried out.

We report that a major voltage-dependent Ca^{2+} channel in dog basilar artery smooth muscle was LVA (activation at –52 mV in 10 mM Ba^{2+} and –51 mV in 10 mM Ca^{2+}). LVA currents are believed to be carried by T-type Ca^{2+} channels that have activation thresholds between –45 mV (Klockner *et al.* 1999) and –70 mV (Serrano *et al.* 1999) in physiological Ca^{2+}, which is consistent with currents observed here. Also consistent with T-type channel current, LVA current was 179- to 637-fold less sensitive to the dihydropyridine nimodipine than HVA current (Petkov *et al.* 2001). This current activated and inactivated voltage dependently and relatively rapidly ($\tau_R = 2.9$ ms and τ_{F1} for maximum peak current ~160 ms), resulting in a criss-crossing pattern of current traces characteristic of T-type channels (Klockner *et al.* 1999; Petkov *et al.* 2001; Perez-Reyes, 2003). Deactivation was slower ($\tau \approx 5.5$ ms) and voltage dependent, with τ increasing with less negative repolarization as previously described for T-type current (Serrano *et al.* 1999; Klockner *et al.* 1999). The voltage dependence and temporal characteristics most closely resemble currents carried by $Ca_{v3.3}$ channels (Klockner *et al.* 1999; Frazier *et al.* 2001; Catterall *et al.* 2005). $Ca_{v3.1}$ and $Ca_{v3.2}$ subtypes have 3- to 5-times more rapid activation and deactivation and are most readily distinguished from $Ca_{v3.3}$ by more rapid inactivation (Catterall *et al.* 2005). Inactivation observed here ($\tau = 164$ ms in 10 mM Ba^{2+} and 177 ms in 10 mM Ca^{2+}) most closely matches that reported for $Ca_{v3.3}$ (Klockner *et al.* 1999; Frazier *et al.* 2001; Catterall *et al.* 2005). We confirmed this by identifying mRNA and protein for $Ca_{v3.3}$ α_1 subunit in dog basilar artery and localizing this to the smooth muscle cells by confocal microscopy. Furthermore, suppression of basal tone and relaxation of arteries contracted *in vitro* by mibefradil, a putative T-type Ca^{2+} channel antagonist, also supports the presence of these channels, although our electrophysiological results suggest that mibefradil is not very specific (Bezprozvanny & Tsien, 1995). There also was a prominent window current in the voltage range around resting V_m (Weyer *et al.* 2005). Our isometric tension recordings of basilar arteries *in vitro* suggest that some LVA current exists and is functionally important.

While some early publications suggested that coronary, renal, aortic and mesenteric artery smooth muscle, as well as rabbit ear and rat tail artery, might possess a LVA current (Bean *et al.* 1986; Ganitkevich & Isenberg, 1990; Smirnov & Aaronson, 1992), other investigators could not demonstrate it (Quignard *et al.* 2001; Ishiguro *et al.* 2005) and the exact nature of the current was uncertain, especially in view of reports of non-L-type HVA currents in some vascular beds, such as the kidney (Hansen *et al.* 2000). Furthermore, it was never well described in the cerebral circulation. Electrophysiological and mRNA data confirm that some arterial smooth muscle expresses T-type channels (Hansen *et al.* 2001; Gustafsson *et al.* 2001). We provide the first documentation of T-type channels in large arteries of the cerebral circulation. Immunohistochemical staining for $Ca_{v3.1}$ protein was reported in penetrating arterioles in rat brain but staining in large arteries was not commented upon and electrophysiological evidence of function was not provided (Brueggemann *et al.* 2005). One limitation is that we were not able to detect a third isoform of T-type channels ($Ca_{v3.2}$) due to lack of antibody reactivity (Perez-Reyes, 2003).

Our experiments confirm L-type, HVA current in dog basilar artery. This is based on electrophysiology as well as the presence of mRNA and protein for α_1 subunits of L-type channels in smooth muscle cells. The current activated at approximately –30 mV, reached a maximum at +20 mV and inactivated slowly in a voltage-dependent manner, with a τ of the order of seconds ($\tau_{F2} = 1244 \pm 81$ ms). Deactivation was of the order of 1 ms and was not voltage dependent. All of these features are common for currents conducted by Ca^{2+} channels of the L-type in a variety of expression systems and cells (Simard, 1991; Janssen, 1997; Petkov *et al.* 2001; Hollywood *et al.* 2003). These cells contained mRNA for L-type ($Ca_{v1.1}$, $Ca_{v1.2}$ and $Ca_{v1.3}$) and protein for L-type ($Ca_{v1.2}$ and $Ca_{v1.3}$) Ca^{2+} channel α_1 subunits. Antibodies for $Ca_{v1.1}$ are not available so we cannot determine if protein for this subunit is present. It is likely, however, that it is not functional because Ca^{2+} currents carried by $Ca_{v1.1}$ subunits have a more positive activation threshold (+8 to +14 mV), a low rate of activation (> 50 ms) and do not display Ca^{2+}-dependent inactivation, which distinguishes them from $Ca_{v1.2}$ and $Ca_{v1.3}$ and from those shown in the present study (Catterall *et al.* 2005). Nimodipine inhibited basal tension and KCl-induced contraction of intact arteries which supports a role for L-type channels.

Our results suggest that there are N-type channels in dog basilar artery smooth muscle. Electrophysiological data showed a small but statistically significant HVA current inhibition by ω-conotoxin GVIA ($\gamma 1\ \mu$M), a specific N-type channel antagonist (Olivera *et al.* 1994). mRNA and protein for this channel were present in smooth muscle

cells. On the other hand, we were unable to demonstrate effect of ω-conotoxin GVIA on intact artery segments so the contribution of this channel to contraction seems minimal. It is likely that these channels are present though because they are reported to have an activation threshold of +10 mV and a potential of half-inactivation between –60 and –70 mV (Williams *et al.* 1994; Stea *et al.* 1999). Thus, they are good candidates for the current we observed as a hump at $V_m = +20$ mV on the difference current curve (Fig. 1*C*).

A second major finding was that cells with varying components of HVA and LVA currents were identified. Inhomogeneity of responses has been noted in other smooth muscles. Janssen (1997) described T- and L-type currents in dog bronchial smooth muscle and noted that there were cells with only HVA current and with HVA plus LVA but none with LVA current alone. Other smooth muscles may have cells with differing voltage-dependent Ca^{2+} channel distributions (Ganitkevich & Isenberg, 1990; Smirnov & Aaronson, 1992; Gordienko *et al.* 1994; Petkov *et al.* 2001). Protein for different α subunits was identified in intact smooth muscle cells which makes it unlikely that variations in the currents present were due to selective isolation of cells from the artery or damage to the cells during isolation. It is tempting to speculate that cells with different Ca^{2+} channel currents have different functions. Cells with predominately LVA currents may be responsible for spontaneous rhythmic activity of cerebral arteries, as has been observed in rabbit basilar artery (Omote & Mizusawa, 1996). Furthermore, the putative role of L-type channels in Ca^{2+} sparklets in cerebral arteries also needs to take into consideration that other voltage-dependent Ca^{2+} channels may be present in these arteries (Navedo *et al.* 2005).

While the electrophysiological and mRNA data document the presence of T- and L-type Ca^{2+} channels, the effects of antagonists of these channels were less specific than might be expected. Mibefradil, a putative T-type channel antagonist, antagonized HVA currents 5-fold more effectively than LVA currents with step protocols and equally effectively using ramp protocols. T-type currents also displayed some sensitivity to nimodipine, similar to the sustained LVA current in pyramidal neurons (Avery & Johnston, 1996). Mibefradil blocked Ca^{2+} currents due to $Ca_{v2.1}$, $Ca_{v2.2}$, $Ca_{v1.2}$ and $Ca_{v2.3}$ (corresponding to P/Q-, N-, L- and R-type) at 10–100 μM and T-type at around 10 nM (Bezprozvanny & Tsien, 1995; Hansen *et al.* 2001). The present results show no differential effect, perhaps due to the presence of multiple Ca^{2+} channel currents.

We also used a different approach to analysis of antagonist data to try to separate current types based on the sensitivity to an antagonist at different voltages (Fig. 6). Current–voltage characteristics of Ca^{2+} channel currents in the presence of nimodipine or mibefradil plotted by this method suggested that current conducted by HVA channels was of two types that differ in affinity for these antagonists and that are activated at voltages of –20 and –5 mV. One or possibly two types of channels mediate current at a low voltage range of activation. This analysis also readily shows that low concentrations (0.01 μM) of nimodipine and mibefradil increased I_{Ba} at voltages below –20 mV, another characteristic of T-type Ca^{2+} channels (Oike *et al.* 1990; Avdonin *et al.* 2000; Xi & Angus, 2001). It does not, however, exclude the possibility of opening of non-selective cation channels, similar to leak channels in skeletal muscle that are activated by nifedipine (Alderton & Steinhardt, 2000). It also is possible that non-linear effects could be due to voltage- and/or concentration-dependent antagonism, that the inhibitors are partitioning in the membrane or influencing other proteins that modulate HVA or LVA currents indirectly or that the inhibitors antagonize other channels.

We provide evidence of physiological significance of the channels we identified. We identified window currents for both HVA and LVA currents. Ba^{2+} was the charge carrier and under physiological conditions the position of the activation and inactivation curves as well as relative magnitudes of currents will be different (Smirnov & Aaronson, 1992; Langton & Standen, 1993). Ba^{2+} shifts activation ~20 mV positive and increases the relative magnitude of L-type current. Second, the V_m at which the smooth muscle exists *in vivo* is not known exactly. We reported that pressurized dog basilar artery smooth muscle at body temperature had a resting V_m of ~30 mV (Weyer *et al.* 2005). The actual value *in vivo* may be more negative. Taking these factors into account, the LVA current would and the HVA current may exhibit substantial window current *in vivo*. Second, isometric tension recordings *in vitro* showed significant effects of antagonists to each channel subtype.

This characterization of voltage-dependent Ca^{2+} channels in dog basilar artery is an important first step in understanding the physiology of this artery as well as forming a basis upon which to study the pathophysiology of vasospasm or contraction of this artery that occurs after subarachnoid hemorrhage (SAH) since the dog is a commonly used species in which to model SAH and is accepted to be one of the best models (Megyesi *et al.* 2000). Theories that vasospasm is associated with an increased function and/or expression of Ca^{2+} channels soon after SAH (Debdi *et al.* 1993) and that this is decreased later (Kamata *et al.* 1991; Yamada *et al.* 1994) can now be tested.

References

Aaronson PI, Bolton TB, Lang RJ & MacKenzie I (1988). Calcium currents in single isolated smooth muscle cells from the rabbit ear artery in normal-calcium and high-barium solutions. *J Physiol* **405**, 57–75.

Alborch E, Salom JB & Torregrosa G (1995). Calcium channels in cerebral arteries. *Pharmacol Ther* **68**, 1–34.

Alderton JM & Steinhardt RA (2000). Calcium influx through calcium leak channels is responsible for the elevated levels of calcium-dependent proteolysis in dystrophic myotubes. *J Biol Chem* **275**, 9452–9460.

Avdonin PV, Buhler FR & Tkachuk VA (2000). Ca^{2+}-agonistic effect of a T-type Ca-channel blocker mibefradil (Ro40-5967). *Membr Cell Biol* **13**, 645–655.

Avery RB & Johnston D (1996). Multiple channel types contribute to the low-voltage-activated calcium current in hippocampal CA3 pyramidal neurons. *J Neurosci* **16**, 5567–5582.

Bean BP, Sturek M, Puga A & Hermsmeyer K (1986). Calcium channels in muscle cells isolated from rat mesenteric arteries: modulation by dihydropyridine drugs. *Circ Res* **59**, 229–235.

Benham CD, Hess P & Tsien RW (1987). Two types of calcium channels in single smooth muscle cells from rabbit ear artery studied with whole-cell and single-channel recordings. *Circ Res* **61**, I10–I16.

Bezprozvanny I & Tsien RW (1995). Voltage-dependent blockade of diverse types of voltage-gated Ca^{2+} channels expressed in Xenopus oocytes by the Ca^{2+} channel antagonist mibefradil (Ro40-5967). *Mol Pharmacol* **48**, 540–549.

Brueggemann LI, Martin BL, Barakat J, Byron KL & Cribbs LL (2005). Low voltage-activated calcium channels in vascular smooth muscle: T-type channels and AVP-stimulated calcium spiking. *Am J Physiol Heart Circ Physiol* **288**, H923–H935.

Buljubasic N, Flynn NM, Marijic J, Rusch NJ, Kampine JP & Bosnjak ZJ (1992). Effects of isoflurane on K^+ and Ca^{2+} conductance in isolated smooth muscle cells of canine cerebral arteries. *Anesth Analg* **75**, 590–596.

Catterall WA, Perez-Reyes E, Snutch TP & Striessnig J (2005). International Union of Pharmacology. XLVIII. Nomenclature and structure-function relationships of voltage-gated calcium channels. *Pharmacol Rev* **57**, 411–425.

Cohen CJ & McCarthy RT (1987). Nimodipine block of calcium channels in rat anterior pituitary cells. *J Physiol* **387**, 195–225.

D'Ascenzo M, Vairano M, Andreassi C, Navarra P, Azzena GB & Grassi C (2004). Electrophysiological and molecular evidence of L-(Ca_{v1}), N-($Ca_{v2.2}$), and R-($Ca_{v2.3}$) type Ca^{2+} channels in rat cortical astrocytes. *Glia* **45**, 354–363.

Day ML, Johnson MH & Cook DI (1998). Cell cycle regulation of a T-type calcium current in early mouse embryos. *Pflugers Arch* **436**, 834–842.

Debdi M, Seylaz J & Sercombe R (1993). Increased influence of calcium and nicardipine on rabbit basilar artery reactivity after brief subarachnoid hemorrhage. *J Cardiovasc Pharmacol* **21**, 754–759.

Findlay I (2002). Voltage- and cation-dependent inactivation of L-type Ca^{2+} channel currents in guinea-pig ventricular myocytes. *J Physiol* **541**, 731–740.

Frazier CJ, Serrano JR, George EG, Yu X, Viswanathan A, Perez-Reyes E & Jones SW (2001). Gating kinetics of the α1I T-type calcium channel. *J General Physiol* **118**, 457–470.

Ganitkevich VY & Isenberg G (1990). Contribution of two types of calcium channels to membrane conductance of single myocytes from guinea-pig coronary artery. *J Physiol* **426**, 19–42.

Glassmeier G, Hauber M, Wulfsen I, Weinsberg F, Bauer CK & Schwarz JR (2001). Ca^{2+} channels in clonal rat anterior pituitary cells (GH3/B6). *European J Physiol* **442**, 577–587.

Gordienko DV, Clausen C & Goligorsky MS (1994). Ionic currents and endothelin signaling in smooth muscle cells from rat renal resistance arteries. *Am J Physiol* **266**, F325–F341.

Gustafsson F, Andreasen D, Salomonsson M, Jensen BL & Holstein-Rathlou N (2001). Conducted vasoconstriction in rat mesenteric arterioles: role for dihydropyridine-insensitive Ca^{2+} channels. *Am J Physiol Heart Circ Physiol* **280**, H582–H590.

Han W, Bao W, Wang Z & Nattel S (2002). Comparison of ion-channel subunit expression in canine cardiac purkinje fibers and ventricular muscle. *Circ Res* **91**, 790–797.

Hansen PB, Jensen BL, Andreasen D, Friis UG & Skott O (2000). Vascular smooth muscle cells express the alpha (1A) subunit of a P-/Q-type voltage-dependent Ca^{2+} channel, and it is functionally important in renal afferent arterioles. *Circ Res* **87**, 896–902.

Hansen PB, Jensen BL, Andreasen D & Skott O (2001). Differential expression of T- and L-type voltage-dependent calcium channels in renal resistance vessels. *Circ Res* **89**, 630–638.

Hille B (2001). *Ion Channels of Excitable Membranes*, 3rd edn. Sinauer Associates, Sunderland, MA.

Hollywood MA, Cotton KD, Thornbury KD & McHale NG (1997). Tetrodotoxin-sensitive sodium current in sheep lymphatic smooth muscle. *J Physiol* **503**, 13–20.

Hollywood MA, Woolsey S, Walsh IK, Keane PF, McHale NG & Thornbury KD (2003). T- and L-type Ca^{2+} currents in freshly dispersed smooth muscle cells from the human proximal urethra. *J Physiol* **550**, 753–764.

Ishiguro M, Wellman TL, Honda A, Russell SR, Tranmer BI & Wellman GC (2005). Emergence of a R-type Ca^{2+} channel (CaV 2.3) contributes to cerebral artery constriction after subarachnoid hemorrhage. *Circ Res* **96**, 419–426.

Janssen LJ (1997). T-type and L-type Ca^{2+} currents in canine bronchial smooth muscle: characterization and physiological roles. *Am J Physiol* **272**, C1757–C1765.

Jensen LJ, Salomonsson M, Jensen BL & Holstein-Rathlou NH (2004). Depolarization-induced calcium influx in rat mesenteric small arterioles is mediated exclusively via mibefradil-sensitive calcium channels. *Br J Pharmacol* **142**, 709–718.

Kamata K, Nishiyama H, Miyata N & Kasuya Y (1991). Changes in responsiveness of the canine basilar artery to endothelin-1 after subarachnoid hemorrhage. *Life Sci* **49**, 217–224.

Kim N, Han J & Kim E (2003). Effects of prostaglandin F2α on membrane currents in rabbit middle cerebral arterial smooth muscle cells. *Am J Physiol Heart Circ Physiol* **284**, H1018–H1027.

Kim YC, Koh SD & Sanders KM (2002). Voltage-dependent inward currents of interstitial cells of Cajal from murine colon and small intestine. *J Physiol* **541**, 797–810.

Klockner U, Lee JH, Cribbs LL, Daud A, Hescheler J, Pereverzev A, Perez-Reyes E & Schneider T (1999). Comparison of the Ca^{2+} currents induced by expression of three cloned $\alpha 1$ subunits, $\alpha 1$G, $\alpha 1$H and $\alpha 1$I, of low-voltage-activated T-type Ca^{2+} channels. *Eur J Neurosci* **11**, 4171–4178.

Kuga T, Kobayashi S, Hirakawa Y, Kanaide H & Takeshita A (1996). Cell cycle-dependent expression of L- and T-type Ca^{2+} currents in rat aortic smooth muscle cells in primary culture. *Circ Res* **79**, 14–19.

Langton PD & Standen NB (1993). Calcium currents elicited by voltage steps and steady voltages in myocytes isolated from the rat basilar artery. *J Physiol* **469**, 535–548.

Loirand G, Mironneau C, Mironneau J & Pacaud P (1989). Two types of calcium currents in single smooth muscle cells from rat portal vein. *J Physiol* **412**, 333–349.

McCarthy RT & Cohen CJ (1989). Nimodipine block of calcium channels in rat vascular smooth muscle cell lines. Exceptionally high-affinity binding in A7r5 and A10 cells. *J General Physiol* **94**, 669–692.

Megyesi JF, Vollrath B, Cook DA & Findlay JM (2000). In vivo animal models of cerebral vasospasm: a review. *Neurosurgery* **46**, 448–460.

Mogul DJ & Fox AP (1991). Evidence for multiple types of Ca^{2+} channels in acutely isolated hippocampal CA3 neurones of the guinea-pig. *J Physiol* **433**, 259–281.

Morita H, Cousins H, Onoue H, Ito Y & Inoue R (1999). Predominant distribution of nifedipine-insensitive, high voltage-activated Ca^{2+} channels in the terminal mesenteric artery of guinea pig. *Circ Res* **85**, 596–605.

Nakayama S & Brading AF (1993). Inactivation of the voltage-dependent Ca^{2+} channel current in smooth muscle cells isolated from the guinea-pig detrusor. *J Physiol* **471**, 107–127.

Navedo MF, Amberg GC, Votaw VS & Santana LF (2005). Constitutively active L-type Ca^{2+} channels. *Proc Natl Acad Sci U S A* **102**, 11112–11117.

Nelson MT, Patlak JB, Worley JF & Standen NB (1990). Calcium channels, potassium channels, and voltage dependence of arterial smooth muscle tone. *Am J Physiol* **259**, C3–C18.

Nelson MT & Quayle JM (1995). Physiological roles and properties of potassium channels in arterial smooth muscle. *Am J Physiol* **268**, C799–C822.

Ohya Y & Sperelakis N (1989). ATP regulation of the slow calcium channels in vascular smooth muscle cells of guinea pig mesenteric artery. *Circ Res* **64**, 145–154.

Oike M, Inoue Y, Kitamura K & Kuriyama H (1990). Dual action of FRC8653, a novel dihydropyridine derivative, on the Ba^{2+} current recorded from the rabbit basilar artery. *Circ Res* **67**, 993–1006.

Olivera BM, Miljanich GP, Ramachandran J & Adams ME (1994). Calcium channel diversity and neurotransmitter release: the ω-conotoxins and ω-agatoxins. *Annu Rev Biochem* **63**, 823–867.

Omote M & Mizusawa H (1996). Interaction between the L-type Ca^{2+} channel and the Ca^{2+}-activated K^+ channel in the fluctuating myogenic contraction in the rabbit basilar artery. *Jpn J Physiol* **46**, 353–356.

Perez-Reyes E (2003). Molecular physiology of low-voltage-activated t-type calcium channels. *Physiol Rev* **83**, 117–161.

Petkov GV, Fusi F, Saponara S, Gagov HS, Sgaragli GP & Boev KK (2001). Characterization of voltage-gated calcium currents in freshly isolated smooth muscle cells from rat tail main artery. *Acta Physiol Scand* **173**, 257–265.

Platzer J, Engel J, Schrott-Fischer A, Stephan K, Bova S, Chen H, Zheng H & Striessnig J (2000). Congenital deafness and sinoatrial node dysfunction in mice lacking class D L-type Ca^{2+} channels. *Cell* **102**, 89–97.

Quignard JF, Harricane MC, Menard C, Lory P, Nargeot J, Capron L, Mornet D & Richard S (2001). Transient down-regulation of L-type Ca^{2+} channel and dystrophin expression after balloon injury in rat aortic cells. *Cardiovasc Res* **49**, 177–188.

Serrano JR, Perez-Reyes E & Jones SW (1999). State-dependent inactivation of the $\alpha 1$G T-type calcium channel. *J General Physiol* **114**, 185–201.

Simard JM (1991). Calcium channel currents in isolated smooth muscle cells from the basilar artery of the guinea pig. *Pflugers Arch* **417**, 528–536.

Simard JM, Li X & Tewari K (1998). Increase in functional Ca^{2+} channels in cerebral smooth muscle with renal hypertension. *Circ Res* **82**, 1330–1337.

Smirnov SV & Aaronson PI (1992). Ca^{2+} currents in single myocytes from human mesenteric arteries: evidence for a physiological role of L-type channels. *J Physiol* **457**, 455–475.

Stea A, Dubel SJ & Snutch TP (1999). $\alpha 1$B N-type calcium channel isoforms with distinct biophysical properties. *Ann New York Acad Sci* **868**, 118–130.

Sun L, Fan JS, Clark JW & Palade PT (2000). A model of the L-type Ca^{2+} channel in rat ventricular myocytes: ion selectivity and inactivation mechanisms. *J Physiol* **529**, 139–158.

Weyer GW, Jahromi BS, Aihara Y, Agbaje-Williams M, Nikitina E, Zhang ZD & Macdonald RL (2005). Expression and function of inwardly rectifying potassium channels after experimental subarachnoid hemorrhage. *J Cereb Blood Flow Metab* **26**, 382–391.

Williams WE, Marubio LM, Deal CR, Hans M, Brust PF, Philipson LH, Miller RJ, Johnson EC, Harpold MM & Ellis SB (1994). Structure and functional characterization of neuronal $\alpha 1$E calcium channel subtypes. *J Biol Chem* **269**, 22347–22357.

Worley JF, Quayle JM, Standen NB & Nelson MT (1991). Regulation of single calcium channels in cerebral arteries by voltage, serotonin, and dihydropyridines. *Am J Physiol* **261**, H1951–H1960.

Xi Q & Angus JA (2001). Evidence against an action of mibefradil at N-type voltage-operated calcium channels. *Naunyn Schmiedebergs Arch Pharmacol* **364**, 430–436.

Yamada T, Tanaka Y, Fujimoto K, Nakahara N, Shinoda S & Masuzawa T (1994). Relationship between cytosolic Ca^{2+} level and contractile tension in canine basilar artery of chronic vasospasm. *Neurosurgery* **34**, 496–503.

Yatani A, Seidel CL, Allen J & Brown AM (1987). Whole-cell and single-channel calcium currents of isolated smooth muscle cells from saphenous vein. *Circ Res* **60**, 523–533.

Young JB, Jahromi BS, Zhang ZD & Macdonald RL (2006). A novel device for *in vitro* isometric tension recordings of cylindrical artery segments. *Med Eng Phys* **29**, 169–174.

Acknowledgements

This work was supported by grants (to R.L.M.) from the American Heart Association, the National Institutes of Health (NS25946) and the Brain Research Foundation. B.S.J. was supported by the Canadian Institutes of Health Research and the American Association of Neurological Surgeons.